Electronic structure and superconducting properties of lanthanum

Lane W. Nixon,[1] D. A. Papaconstantopoulos,[1] and Michael J. Mehl[2]
[1]*Department of Computational and Data Sciences, George Mason University, Fairfax, Virginia 22030, USA*
[2]*Center for Computational Materials Science, Naval Research Laboratory, Washington, DC 20375, USA*
(Received 7 August 2008; revised manuscript received 16 October 2008; published 18 December 2008)

The total energy and electronic structure of lanthanum have been calculated in the bcc, fcc, hcp, and double hcp structures for pressures up to 35 GPa. The full-potential linearized-augmented-plane-wave method was used with both the local-density approximation (LDA) and generalized-gradient approximation (GGA). The correct phase ordering has been found by the GGA results, with lattice parameters and bulk moduli in good agreement with experimental data. The GGA method shows excellent agreement with experiment while the LDA results show some discrepancies. The calculated strain energies for the fcc and bcc structures demonstrate the respective stable and unstable configurations at ambient conditions. The calculated superconductivity properties under pressure for the fcc structure are also found to agree well with measurements. Both LDA and GGA, with minor differences, reproduce well the experimental results for the superconducting critical temperature T_c.

DOI: 10.1103/PhysRevB.78.214510 PACS number(s): 74.25.Jb, 74.25.Kc, 74.25.Ld, 74.62.Fj

I. INTRODUCTION

Lanthanum, which possesses several interesting and anomalous properties, has been a source of continued study and debate over several decades. At ambient conditions lanthanum takes either the stable α-La double hcp (dhcp) or the metastable β-La fcc structure, and a γ-La bcc structure is favorable at high temperatures near the melting point. The metastable β-La fcc can be made stable if the sample is thin (less than $\frac{1}{8}$ in.), annealed, and rapidly quenched.[1] Otherwise it will revert to the stable dhcp and small anisotropic strains induce the transformation from fcc to dhcp.[2] The dhcp and the stable fcc yield superconducting transition temperatures T_c near 5 and 6 K, respectively, at equilibrium pressure.[3] Both structures show significant increases in T_c with pressure[4] with the dhcp undergoing several structural transformations. The α-La dhcp transforms to the β-La fcc near 2.2 GPa, shifts at about 2.5 GPa to a distorted fcc (dfcc) structure, then returns to the β-La fcc phase near 90 GPa.[5] The stable fcc equilibrium structure, however, shows no structural changes throughout the pressure range of experiment.[6]

Several theoretical works on fcc and dhcp La have focused on the electronic structure of lanthanum since the late 1960s and with an increase in experimental data over extended pressure ranges for both the dhcp and fcc structures. Fleming *et al.*[7] presented band-structure and Fermi-surface results for dhcp La using non-self-consistent relativistic augmented-plane-wave (APW) (RAPW) with the Slater $\rho^{1/3}$ exchange. The next year Myron and Liu[8] used the same method, presenting results for fcc Kmetko,[9] using self-consistent nonrelativistic calculations from the APW method, presented f-electron charge reduction with pressure for fcc La, a result which is contradicted by the finding of our paper. Glötzel and Fritsche[10] presented the variation in the electronic structure of fcc La with pressure from a semirelativistic rigorous cellular method. Glötzel[11] reported the ground-state properties of fcc and dhcp La using self-consistent calculations from the linear-muffin-tin-orbital (LMTO) method with the atomic-sphere approximation (ASA). Takeda and Kubler[12] presented electronic structure results for fcc La using self-consistent semirelativistic linearized augmented-plane-wave (LAPW) calculations with the ASA. Pickett *et al.*[13] reported self-consistent relativistic LAPW band-structure results for fcc La using the Kohn-Sham-Gasper $(\alpha=\frac{2}{3})\rho^{1/3}$ form of the local-density approximation (LDA). McMahan *et al.*[14] investigated the band-structure and s-d transition properties of fcc La with the LMTO method and the von Barth–Hedin[15] (vBH) LDA exchange-correlation potential. Lu *et al.*[16] presented self-consistent LAPW calculations of total energies and electronic structures of fcc and bcc La using the LDA with three different exchange-correlation potentials. Skriver and Mertig[17] performed self-consistent scalar-relativistic LMTO vBH LDA calculations within the ASA to estimate the Hopfield parameter[18] for dhcp La (and other rare earths). Jarlborg *et al.*[2] presented band-structure, Fermi-surface, and superconductivity calculations of fcc and dhcp La using self-consistent scalar-relativistic LMTO. Söderlind *et al.*[19] presented self-consistent scalar-relativistic LMTO elastic constant calculations of cubic f-electron elements. Delin *et al.*[20] reported results of a systematic study of the cohesive properties of the lanthanides using full-potential LMTO LDA and generalized-gradient approximation (GGA) calculations. Recently Gao *et al.*[21] used the ultrasoft Vanderbilt GGA pseudopotential, which neglects the 4f electrons, to determine the elastic constants, phonon frequencies, and electron-phonon coupling constant λ.

In this work we report the results of full-potential self-consistent scalar-relativistic LAPW calculations of the electronic structure and superconductivity properties of several crystal structures of lanthanum as functions of pressure for both the LDA and the GGA methods. In particular, we report the total energies for the following: the bcc, fcc, hcp, and dhcp structures; the elastic constants for the bcc and fcc at equilibrium conditions; the density of states, including spin-orbit interactions, for the fcc and GGA dhcp structures and the band structure for the GGA fcc; the superconducting

properties, with spin-orbit interactions, for the fcc structure through high pressures and for the GGA dhcp structure at the calculated equilibrium; and the phonon spectrum for the GGA fcc structure at equilibrium conditions.

These are to our knowledge another all-electron GGA calculations of the elastic constants, phonon frequencies, and superconductivity properties for this material at high pressures. We found that the best representation of the structural behavior and energetics was obtained using the generalized-gradient approximation. The results from these first-principles calculations were input to the rigid-muffin-tin approximation (RMTA) from Gyorffy and co-workers[22,23] to help explain the pressure-dependent superconducting behavior of the fcc and dhcp structures.

II. THEORY AND COMPUTATIONAL DETAILS

Full-potential self-consistent scalar-relativistic LAPW total-energy[24,25] calculations were performed to establish the relationship between total energy, volume, and pressure for the above crystal structures of lanthanum. In a method similar to Ref. 16, the core states were treated as fully relativistic. The extended $5p$ semicore states were treated as bands together with the $4f$, $5d$, and $6s$ levels within a scalar-relativistic approach. Calculations were also performed to determine the impact of including spin-orbit effects in the valence bands.

A. Total energies

The total energies were iterated to self-consistency where the change in total energy was less than 10^{-5} Ry. A muffin-tin (MT) sphere radius of 2.6 a.u. was used for all structures in the LDA and GGA to ensure fewer than 0.1 electron were found outside the MT sphere. At convergence all structures had less than 0.08 electron outside the MT sphere.

For consistency all structures used the same basis-set cutoff distance $RK_{\max}$ required for the extended pressure fcc T_c calculations, where R is the radius of the muffin-tin sphere and $K_{\max}$ is the reciprocal-lattice vector cutoff. Here $RK_{\max}$ was maintained at 9.0 for all structures and for all volumes. The LAPW basis functions, potentials, and charge densities were all expanded up to $l=9$. All k-point summations were performed with temperature broadening equivalent to 2 mRy. The Brillouin-zone summations over the valence states were performed with 89 fcc, 55 bcc, 57 hcp, and 57 dhcp k points in the irreducible part of the Brillouin zone. We used the Hedin-Lundqvist (HL) (Ref. 26) and the Perdew-Wang (PW) (Ref. 27) exchange-correlation potentials for all respective LDA and GGA calculations.

B. Elastic constants

The mechanical stability of bcc and fcc lanthanum was determined by calculating the elastic constants C_{11}, C_{12}, and C_{44} and the bulk modulus B for the cubic bcc and fcc equilibrium structures. Since the theory and computational procedure for calculating these properties have been discussed in detail by Mehl and co-workers,[28,29] we will only provide a summary of the process.

With three independent elastic constants, we apply an orthorhombic strain e to determine the strained energy E as follows:

$$E = E_0 + V(C_{11} - C_{12})e^2 + O[e^4], \tag{1}$$

where E_0 is the unstrained energy and V is the volume of the unit cell which remains constant. The strain energies E were calculated using the procedure for total-energy calculations described above with 341 and 336 k points for bcc $C_{11}-C_{12}$ and C_{44}. The fcc $C_{11}-C_{12}$ and C_{44} had 365 and 333 k points, respectively. The slope or E vs e^2 from Eq. (1) gives the tetragonal shear modulus $C_{11}-C_{12}$. The shear elastic constant C_{44} was determined in a similar fashion with

$$E = E_0 + \frac{1}{2}VC_{44}e^2 + O[e^4], \tag{2}$$

using a volume conserved orthorhombic strain e. The C_{11} and C_{12} were determined by combining the tetragonal shear modulus from Eq. (1) with the relation for the bulk modulus,

$$B = \frac{1}{3}(C_{11} + 2C_{12}). \tag{3}$$

A cubic material is stable if the bulk modulus B, tetragonal shear modulus $C_{11}-C_{12}$, and elastic constant C_{44} are all greater than zero.[30]

C. Densities of states

The density of states (DOS) for fcc and dhcp was calculated by the tetrahedron method[31] using the converged self-consistent scalar-relativistic charge density for touching MT spheres with the $RK_{\max}$ increased to 10.0. Touching MT spheres were used to obtain more accurate angular-momentum components of the DOS and to maintain consistency with the RMTA discussed in Sec. II D. The fcc density of states at ϵ_F was calculated using the tetrahedon method with 89 k points.

The dhcp $N(\epsilon_F)$ were determined by the method proposed by Gillan[32] where the density of states is replaced by a sum of smooth functions centered at eigenvalues of irreducible k points. The 2 mRy Fermi temperature, which was used to determine the total energies, was also used to give weight to each broadening function centered at an energy eigenvalue within the dense k-point mesh. The weighted dhcp density of states was calculated as the sum of the product of energy eigenvalues and matrix elements from 1953 k points in the irreducible Brillouin zone.

D. Superconductivity

From our density of states results at the Fermi level we determine, from first principles, the electron-phonon coupling constant λ and the superconducting transition temperature T_c. Using McMillan's strong-coupling theory,[23,33] we take the electron-phonon coupling constant by the following formula:

$$\lambda = \frac{\eta}{M\langle\omega^2\rangle}, \tag{4}$$

where M is the atomic mass, η is the Hopfield parameter[18] calculated with the RMTA,[22,23] $N(\epsilon_F)$ is the total density of states at the Fermi level, ϵ_F, $\langle I^2\rangle$ is the square of the electron-ion matrix element at ϵ_F, and $\langle\omega^2\rangle$ is the square of the average phonon frequency. The Hopfield parameter[18] is determined by the quantity

$$\eta = N(\epsilon_F)\langle I^2\rangle, \tag{5}$$

using the RMTA. The square matrix element $\langle I^2\rangle$, which is derived from multiple-scattering theory and is also determined by the RMTA prescribed by Gaspari and Gyorffy,[22] is defined by the formula

$$\langle I^2\rangle = \frac{\epsilon_F}{\pi^2 N^2(\epsilon_F)} \Sigma_l \frac{2(l+1)\sin^2(\delta_{l+1}-\delta_l)N_l N_{l+1}}{N_l^{(1)} N_{l+1}^{(1)}}, \tag{6}$$

where δ_l are scattering phase shifts, $N_l(\epsilon_F)$ is the lth component of the DOS per spin, and $N_l^{(1)}$ is the free-scatter DOS. Equation (6) is used with touching MT spheres to minimize errors due to the excess interstitial volume as demonstrated in Refs. 34 and 35 for other third column elements. The LAPW total-energy results were used to calculate the pressure variation in the bulk moduli B. These values were used to determine the average phonon frequency from the volume variation in the bulk modulus, using the following relation:[36]

$$\langle\omega^2\rangle = cB(V)V^{1/2}, \tag{7}$$

where the constant of proportionality c is calculated by equating Eq. (7) with the Debye-type approximation,

$$\langle\omega^2\rangle = \frac{1}{2}\theta_D^2, \tag{8}$$

using the ambient bulk modulus B, volume V, and Debye-temperature θ_D values. The superconductivity transition temperature is given by the McMillan equation,[33]

$$T_c = \frac{\langle\omega\rangle}{1.2}\exp\left[\frac{-1.04(1+\lambda)}{\lambda-\mu*(1+0.62\lambda)}\right], \tag{9}$$

where the Coulumb pseudopotential $\mu*$ was fixed to 0.13 for both the fcc and dhcp structures.

III. RESULTS

A. Total energies

In Fig. 1 we show the LDA total energy of La with respect to the fcc lattice as a function of volume. The symbols represent the LDA values and the lines are the third-order Birch fit. The equilibrium dhcp, which is slightly higher than the fcc, is not predicted as the ground state. The transition from dhcp to fcc at about −1.6 GPa is almost 4 GPa below the transition pressure of 2.2 GPa from experiment.[5] The calculated LDA and experimental equilibrium lattice constants and bulk moduli can be seen in Table I where we also compare with other calculations.

Our calculated bcc and fcc equilibrium lattice constants are in good agreement with all other LDA results, underestimating experiment by about 4.6%. Our calculated bulk moduli agree well with previous Hedin-Lundqvist LDA results.[26]

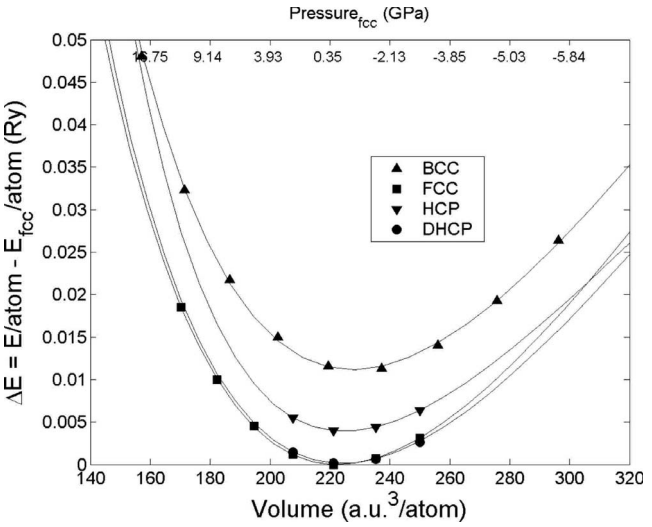

FIG. 1. Lanthanum LDA total energy relative to third-order Birch fit to fcc structure.

For the fcc the LMTO von Barth–Hedin[15] results from McMahan *et al.*[14] shown in the first row of Table I provide the best estimate of the bulk modulus. Their value is just over 3% below experiment. However, their lattice constant, which is about 4% smaller than experiment, is worse than the LMTO ASA calculation from Glötzel,[11] which is about 2.4% below experiment. The LMTO ASA bulk modulus, however, is about 13% above experiment. This is better than the bulk modulus of the Wigner LDA from Ref. 16 of 29.3 GPa or 18% above experiment. The Wigner, however, yields a better approximation of the fcc equilibrium lattice constant with a discrepancy of about 2% below experiment. The lattice constants and bulk moduli from the two $X\alpha$ LDA in Ref. 16 show the best overall agreement with experiment. Our fcc equilibrium lattice constant is about the same as for the HL LDA (Ref. 16) and the LMTO LDA (Ref. 20) at about 4% below experiment. Yet our bulk modulus overestimates the experiment by more than 27%.

The $X\alpha$ with $\alpha=\frac{2}{3}$ and the $5p$ states in the valence exactly matches experiment for the bcc equilibrium lattice while the Wigner LDA and the HL LDA follow with discrepancies of about 2.1% and 4.5% below experiment, respectively. Our bcc results are only slightly different than the HL LDA calculations from Ref. 16, and our LDA dhcp bulk modulus and equilibrium lattice constants, which are closer to experiment than either the LDA fcc or bcc calculations, show significantly more discrepancy than the dhcp calculations using the GGA.

Our GGA total energy of La with respect to the dhcp lattice is shown in Fig. 2 as a function of volume. (A third-order Birch fit was used for all structures except the hcp to determine the equilibrium lattice constant and bulk modulus. A fourth-order Birch fit was used for the hcp.) The phase ordering agrees with experiment showing dhcp as the ground state, but the dhcp to fcc transition pressure, like that for LDA, conflicts with experiment. Here the transition is near 8

TABLE I. Calculated and experimental lattice constants and bulk moduli of bcc, fcc, and dhcp lanthanum. (HL denotes Hedin-Lundqvist, LMTO denotes linearized muffin-tin-orbital, PW denotes Perdew-Wang, Wig. denotes Wigner, $X\alpha$ denotes Kohn-Sham $X\alpha(\alpha=\frac{2}{3})$, and PP denotes Vanderbilt pseudopotential.)

	bcc		fcc		dhcp		
Method	Lattice const. a (bohr)	Bulk modulus (GPa)	Lattice const. a (bohr)	Bulk modulus (GPa)	Lattice const. a (bohr)	Lattice const. c (bohr)	Bulk modulus (GPa)
LMTO LDA[a]			9.65	24.0			
LMTO LDA[b]			9.77	28.0			
LMTO LDA[c]			9.63	27.5			
$X\alpha$ LDA[d]			9.83	13.9			
$X\alpha$ LDA[e]	8.05	27.2	10.06	26.1			
Wig. LDA[f]	7.88	29.0	9.83	29.3			
HL LDA[e]	7.69	31.1	9.60	31.1			
HL LDA[g]	7.69	30.94	9.62	31.5	6.84	22.07	30.0
LMTO GGA[c]			9.8	27.5			27.5
PP GGA[h]			10.10	26.6			
PW GGA[g]	8.01	27.02	10.03	24.8	7.15	23.06	24.39
Expt.	8.05[i]		10.02[i]	24.8[j]	7.13[i]	22.83[i]	24.3[k]

[a]Reference 11.
[b]Reference 14.
[c]Reference 20.
[d]Reference 16, 5p states in core.
[e]Reference 16, 5p states in valence.
[f]Reference 16.
[g]Present work, 5p states in valence.
[h]Reference 21, 4f states omitted from pseudopotential.
[i]Reference 37, dhcp bulk modulus from ideal volume 250 a.u.^{3}.
[j]Reference 38.
[k]Reference 39.

GPa or almost 6 GPa above experiment. Still the calculated lattice constants and bulk moduli, in particular, agree remarkably well with experiment and with the GGA pseudopotential results from Gao *et al.*[21] These GGA and experimental values are also shown in Table I.

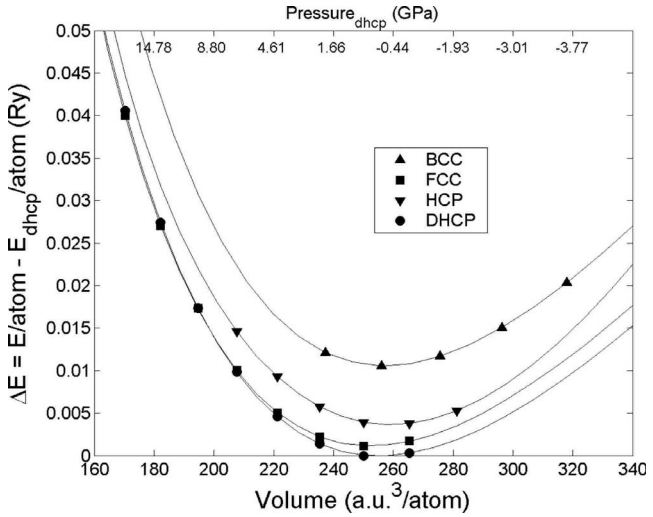

FIG. 2. Lanthanum GGA total energy relative to third-order Birch fit to dhcp structure (fourth-order Birch fit for GGA hcp).

The bcc and fcc equilibrium lattice constants and bulk moduli are comparable to $X\alpha$ LDA. Our Perdew-Wang GGA calculation[27] overestimates the experimental fcc lattice constant of 10.02 a.u. by less than 0.1%. The Vanderbilt GGA pseudopotential, which omits 4f electrons, did almost as well with the second best estimate of the lattice constant and bulk modulus. The LMTO PW GGA from Delin *et al.*[20] provided the worst estimates of the lattice constants and bulk moduli. The estimate of the fcc lattice parameter was acceptable at less than 2% below experiment, but the bulk moduli for the fcc and dhcp were much less in line with experiment. Both bulk moduli were just over 10% above experiment. The bcc equilibrium lattice constant of 8.05 a.u. is underestimated by less than 0.6% by our PW GGA. Our calculated dhcp equilibrium lattice constants are less than 0.6% above experiment, and both the fcc and dhcp bulk moduli are each less than 0.4% more than experiment. Thus, we conclude that our LAPW GGA results yield the best overall agreement with experiment.

B. Elastic constants

The LDA and GGA strain energies for the bcc and fcc were calculated using the same lattice distortions. These energies which are used as input to Eqs. (1) and (2) are shown

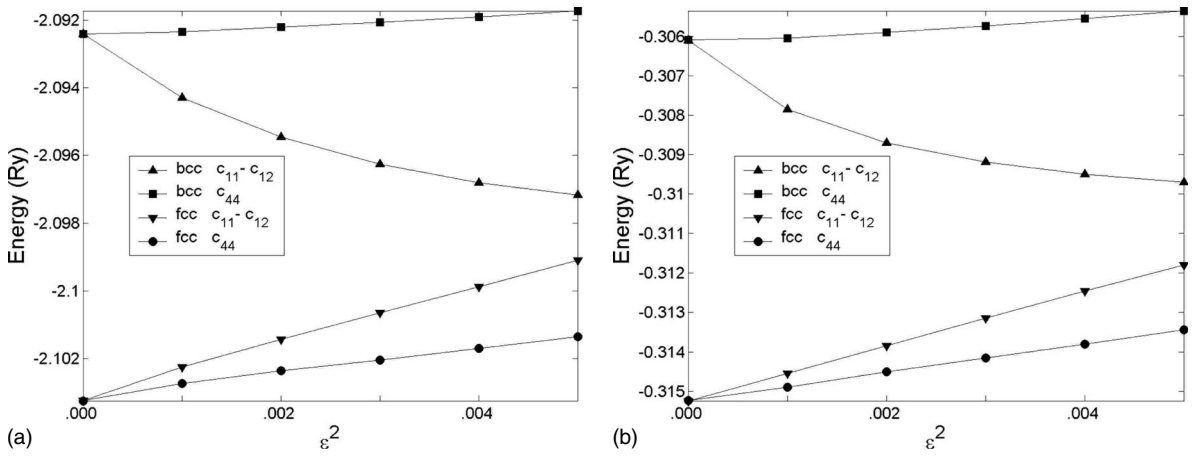

FIG. 3. LDA and GGA strain energies of bcc and fcc at calculated equilibrium volume.

in Fig. 3. The bulk moduli for Eq. (3) are shown in Table I. The calculated elastic constants for the bcc and fcc structures are compiled in Table II. For our LDA we see that the theoretical values for fcc C_{12} are closer to experiment than our GGA yet the C_{11} and C_{44} agree less favorably than do our results for the same GGA constants. But the LMTO LDA fcc constants from Söderlind *et al.*[19] show the opposite trend with the C_{12} below experiment and both C_{11} and C_{44} between the equivalent values for stable and metastable results. As a whole, the GGA fcc results are in very good agreement with both the stable and metastable experimental results.

Our GGA fcc C_{44} constant is between the stable and metastable in value. The C_{11} and C_{12} for the GGA fcc are, respectively, above and below experiment. These elastic constants tend to compensate deviations between themselves and the bulk modulus. The same constants reported by Gao *et al.*[21] were greater than experiment. The experimental bulk moduli are approximately 25.1 GPa for the metastable fcc and 23.1 GPa for the stable fcc. Our calculated GGA fcc bulk modulus of 24.84 GPa is slightly lower than the 26.59 GPa reported by Gao *et al.*[21] and both results agree best with the experimental metastable fcc bulk modulus. The significant discrepancy in our LDA fcc C_{11} constant is due primarily to the severely overestimated bulk modulus. This discrepancy was about 27.2% above experiment.

The results for the bcc calculations show the LDA and GGA are of the same magnitude and in relative agreement. Yet while the fcc is shown to be stable, having a positive bulk modulus, a positive tetragonal elastic constant $C_{11}-C_{12}$, and a positive shear constant C_{44}, the bcc is classified as unstable. Specifically the elastic constant $C_{11}-C_{12}$ is negative for both the LDA and the GGA.

C. Densities of states

The total and angular-momentum decomposed density of states for the fcc and the dhcp at ambient conditions and for the fcc at a higher pressure of 23.9 GPa are plotted in Fig. 4. The strong peak in the total densities at the Fermi level is primarily due to contributions from *d*-like states. The total density of states shows the dhcp and fcc at ambient conditions has slightly different structure near ϵ_F. The high-pressure fcc shows significant differences in its total and decomposed states compared to both structures at equilibrium.

TABLE II. Calculated and experimental elastic constants of bcc and fcc lanthanum.

	bcc				fcc			
	$C_{11}-C_{12}$ (GPa)	C_{11} (GPa)	C_{12} (GP)	C_{44} (GPa)	$C_{11}-C_{12}$ (GPa)	C_{11} (GPa)	C_{12} (GPa)	C_{44} (GPa)
LDA[a]	−76.95	−20.36	56.59	0.39	37.62	56.62	19.00	20.88
LDA[b]					12.8	29.4	16.6	16.8
GGA[a]	−69.75	−19.48	50.27	1.61	20.76	38.68	17.92	17.67
GGA[c]					20.4	42.8	22.4	17.8
Expt.[d]					14.09	34.47	20.38	17.96
Expt.[e]					8.05	28.46	20.41	16.53

[a]Present work, LAPW method.
[b]Reference 19, linearized muffin-tin orbital with 4*f* electrons.
[c]Reference 21, Vanderbilt pseudopotential without 4*f* electrons.
[d]Reference 40, metastable fcc.
[e]Reference 41, stable fcc.

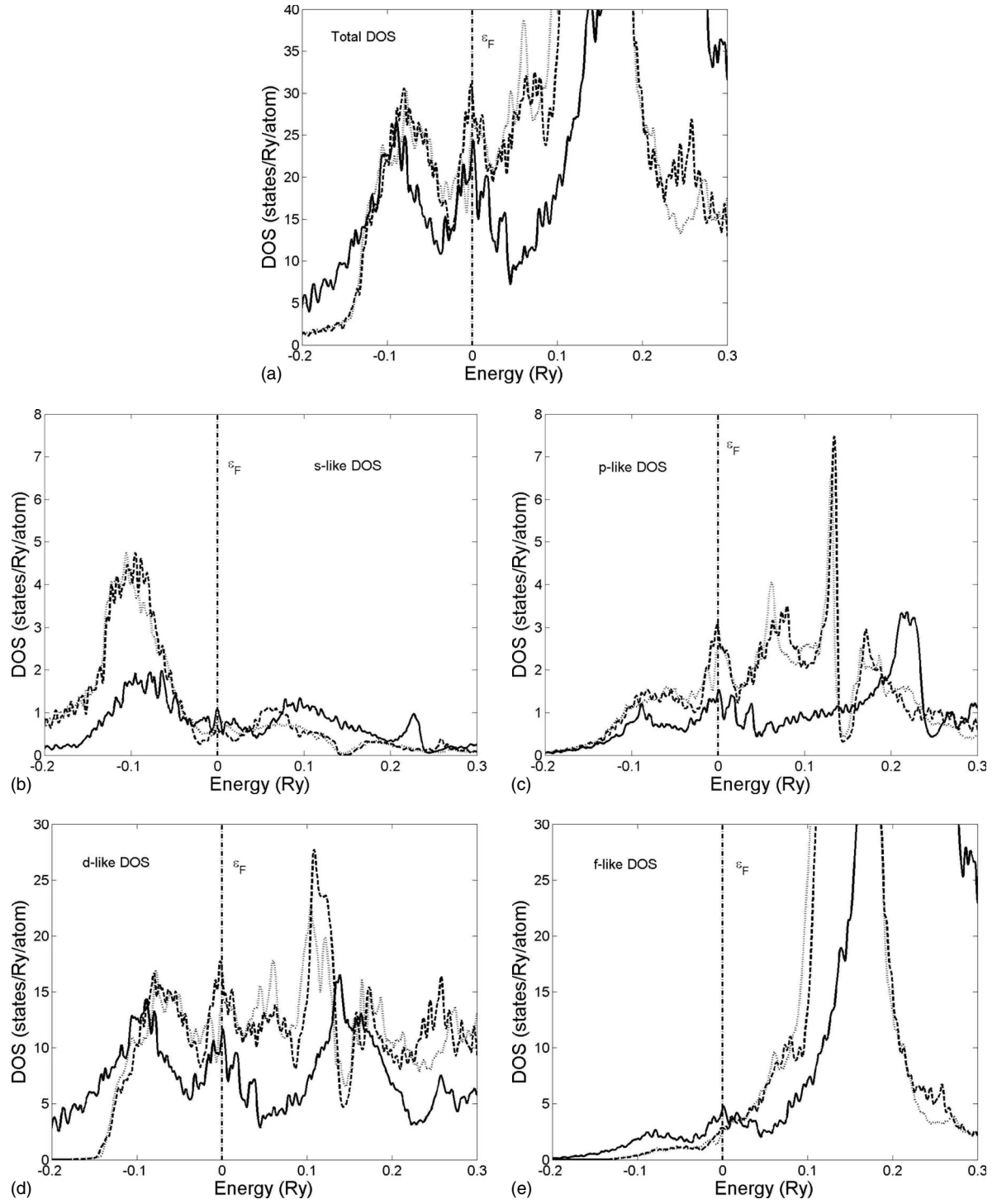

FIG. 4. Total density of states and angular-momentum decompositions of GGA fcc and GGA dhcp La under normal pressure and fcc La under high pressure. The solid, dashed, and dotted lines denote the fcc at 23.9 GPa, the fcc at ambient pressure, and the ambient dhcp, respectively. The dashed-dotted line designates the Fermi level.

The high-pressure fcc exhibits fewer states at the Fermi level and the two dominant f peaks located between 0.1 and 0.2 Ry are at higher energy and are significantly reduced. Our f bands dominate the densities of states at about the same energy, 2–3 eV above ϵ_F, as reported in previous works[2,13] and shown in Fig. 6.

The s-like density of states at ϵ_F decreases from the dhcp to the ambient fcc then increase with pressure. The p-like density of states increases from the dhcp to the ambient fcc. The fcc p states decreases with increased pressure. The d-like density of states increases from the dhcp to the ambient fcc. The fcc d states decrease with increased pressure.

TABLE III. Calculated density of states (states/Ry atom) at ϵ_F at equilibrium volume of fcc and dhcp lanthanum.

Method	fcc $N(\epsilon_F)$	dhcp $N(\epsilon_F)$
RAPW LDA[a]	24.8	
RAPW LDA[b]		19.4
LMTO LDA[c]	31.6	
LMTO LDA[d]	31.0	28.9
LMTO LDA[e]		20.5
LAPW LDA[f]	26.0	
LAPW LDA[g]	27.47	
LAPW LDA[h]	31.2	
LAPW LDA[i]	27.93	
LAPW GGA[j]	30.36	25.85

[a]Reference 8, fcc $a=10.011$ a.u.
[b]Reference 7, dhcp APW sphere radius=3.320 a.u.
[c]Reference 11, fcc $a=10.0348$ a.u.
[d]Reference 2, unspecified fcc; dhcp $c/a=3.225$.
[e]Reference 17, dhcp $c/a=3.230$.
[f]Reference 12, fcc $a=10.11$ a.u.
[g]Reference 13, fcc $a=10.0348$ a.u.
[h]Reference 16, fcc $a=10.0378$ a.u.
[i]Present work, fcc $a=9.6175$.
[j]Present work, fcc $a=10.032$; dhcp $c/a=3.225$.

The f-like density of states increases from the dhcp to the ambient fcc. The angular-momentum contributions and l-character contributions in the fcc are discussed below.

Our total density of states at ϵ_F at equilibrium pressure for fcc and dhcp, as shown in Table III, agrees well with previous calculations. We note, however, that the non-self-consistent RAPW fcc and dhcp results from Myron and Liu[8] and Fleming *et al.*[7] report values for the respective fcc and dhcp $N(\epsilon_F)$ which are lower than our calculations. Using our GGA fcc $N(\epsilon_F)=30.11$ states/Ry/atom and our GGA equilibrium volume fcc electron-phonon coupling constant $\lambda=1.10$ calculated in Sec. III E, we calculate the electronic specific-heat coefficient γ, using the equation $\gamma=0.1734[N(\epsilon_F)(1+\lambda)]$, as 11.0 mJ/(mol K^2), which is about 4.3% below the experimental γ of 11.5 mJ/(mol K^2).[42] Our calculated GGA dhcp γ, using the above equation with $N(\epsilon_F)=25.85$ states/Ry atom and $\lambda=0.83$ from Sec. III E, is 8.2 mJ/(mol K^2), which is just over 13% below the experimental value of 9.45 mJ/(mol K)^2 reported in Ref. 43.

The significant influence of the d-like states at ϵ_F is best viewed in Fig. 5(a), which shows the ratio $N(\epsilon_F)_l/N(\epsilon_F)$ as a function of pressure. The dominant d-like states decrease with pressure from about 72% contribution at zero pressure to about 59% at 30.6 GPa. The f-like states at ϵ_F increase with pressure from 12% to 26.5% at 30.6 GPa. The s-like states at ϵ_F have a small contribution and remain about constant with pressure, and the p-like contribution at ϵ_F decreases with pressure from near 13% at equilibrium to about 8% at 30.6 GPa. These trends agree well with the LDA results from Pickett *et al.*[13]

Our GGA calculations yield slightly higher values of $N(\epsilon_F)$ than LDA. The contribution of the fractional angular-momentum decomposed density of states at ϵ_F at fcc and dhcp equilibrium volumes is displayed in Table IV, with minor differences between the different methods.

The scalar-relativistic LMTO results from Jarlborg *et al.*[2] show slightly higher s- and p-like contributions and slightly lower d-like contributions for both the fcc and dhcp calculations. Our GGA fcc results are comparable to the LDA results from Pickett *et al.*[13] with slightly more p-like decomposed DOS contribution and slightly less d-like contribution. In the dhcp our p-like contributions are lower than the LMTO results from either Jarlborg *et al.*[2] or Skriver and Mertig[17] and our d-like contributions are the highest of the three theoretical results.

The distribution of electrons up to the Fermi level is displayed in Fig. 5(b) as fractional l character of electrons of the GGA fcc as a function of pressure. The dominant d-electron contribution increases from about 69% at equilibrium to about 73% near 24 GPa and decreases thereafter. The contribution due to f electrons increases with pressure from 5% to about 20% near 35 GPa. This increase in fcc f-electron charge with pressure, which opposes results from Kmetko,[9] is in qualitative agreement with results from Pickett *et al.*[13] Both the s- and p-electron contributions decrease with pres-

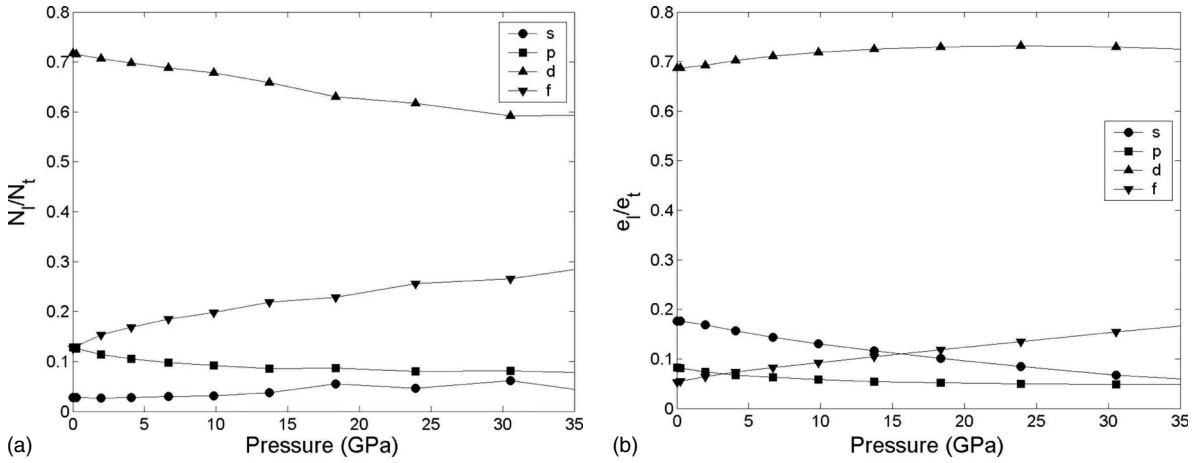

FIG. 5. Angular-momentum decomposed DOS divided by total DOS at ϵ_F and fractional l character of electrons up to ϵ_F as functions of pressure for GGA fcc.

TABLE IV. Calculated fractional angular-momentum decomposed density of states (states/Ry atom) at ϵ_F at equilibrium volume of fcc and dhcp lanthanum.

	fcc				dhcp			
Method	s -like (%)	p -like (%)	d -like (%)	f -like (%)	s -like (%)	p -like (%)	d -like (%)	f -like (%)
LMTO LDA[a]	4	16	67	13	6	17	64	13
LMTO LDA[b]					3	16	68	13
LAPW LDA[c]	3	11	75	11				
LAPW LDA[d]	3	11	70	16				
LAPW GGA[d]	3	13	72	12	4	13	71	12

[a]Reference 2, unspecified fcc; $c/a=3.225$.
[b]Data estimated from Ref. 17, dhcp $c/a=3.230$.
[c]Reference 13, fcc $a=10.0378$ a.u.
[d]Present work, fcc $a=10.032$ a.u.; dhcp $c/a=3.225$.

sure. The s electrons which begin with almost 18% decrease to 6% near 35 GPa and the p-electron contribution decreases from more than 8% to less than 5% near 35 GPa.

D. Band structure and spin-orbit interaction

The change in the band structure of GGA fcc lanthanum at ambient and high pressures is shown in Figs. 6(a) and 6(b), respectively. These results are in qualitative agreement with results from Myron and Liu,[8] Glötzel,[11] Takeda and Kubler,[12] Pickett *et al.*,[13] McMahan *et al.*,[14] and Jarlborg *et al.*[2] The f bands, which are tightly clustered about 0.1 Ry above the Fermi level and entwined with d bands, broaden with pressure but remain well above ϵ_F.

The $5p$ semicore bands, which are the lowest bands in the two plots, are significantly below the Fermi level and broaden with pressure. The lowest d band, which is found as the first band below ϵ_F at the X symmetry point, shifts further below the Fermi level and becomes more occupied with pressure.

The total density of states, with and without spin-orbit interactions, for the GGA fcc at ambient conditions is shown in Fig. 7. The contribution of spin-orbit interaction to the densities of states, particularly at ϵ_F, for either the LDA and GGA is minimal, which agrees well with previous results.[13,21] Our spin-orbit density of states at ϵ_F for the LDA equilibrium fcc is 28.48 states/Ry atom. This value is less than 0.5 states/Ry atom higher than that for the non-spin-orbit LDA. The spin-orbit GGA equilibrium fcc density of states, 30.50 states/Ry atom, at ϵ_F is less than 0.4 states/Ry atom above that without spin-orbit interactions, 30.11 states/Ry atom. Our LDA and GGA calculated equilibrium lattice constants are both slightly lower than those without spin-orbit effects at 9.6175 and 10.0144 a.u., respectively.

The spin-orbit effect on the fcc GGA DOS is negligible as seen in Fig. 7 where the solid line and dotted lines denote the spin-orbit and non-spin-orbit densities of states. However, there is a small but notable difference in the band structure when comparing the original structure seen in Fig. 6(a) and the spin-orbit structure in Fig. 8. The spin-orbit interaction splits the d and f bands located above ϵ_F.

The three triple-degenerate $\Gamma_{25'}$, Γ_{15}, and Γ_{25} bands just above ϵ_F in Fig. 6(a) split to form one double-degenerate and one nondegenerate band in Fig. 8. Since these degenerate bands are above the Fermi level, they add little to either the total energy or the density of states. Yet the effect of spin-orbit interaction cannot be completely ignored at higher pressures when the Fermi level passes through these degeneracies. Thus spin-orbit effects are also considered in our investigation of superconductivity.

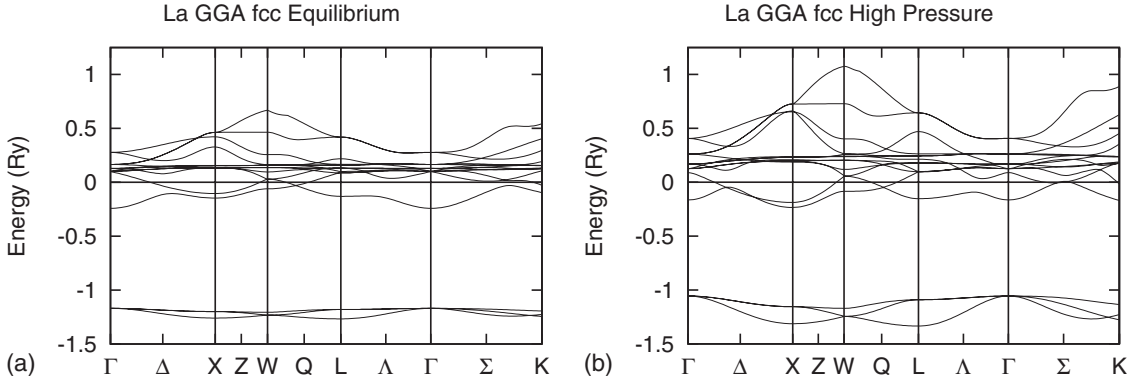

FIG. 6. Band structure of GGA fcc lanthanum.

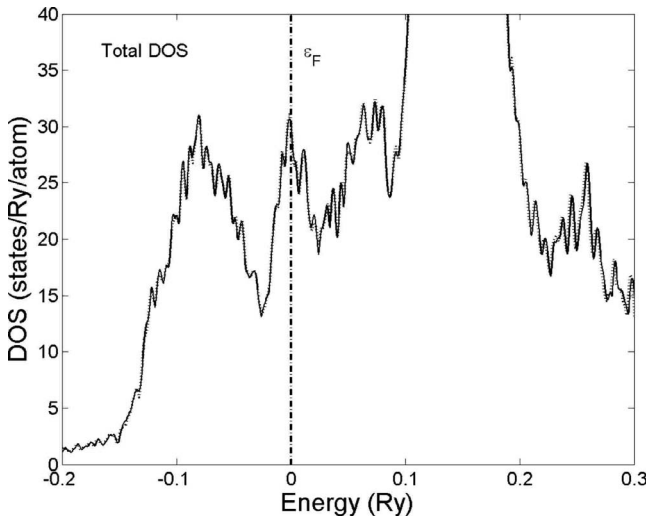

FIG. 7. Total and spin-orbit densities of states of GGA fcc La under normal pressure. The solid and dotted lines essentially overlap and no detectable difference was found. The dashed-dotted line designates the Fermi level.

E. Superconductivity

From our total-energy and density-of-states calculations we determined the input parameters for the T_c calculations for GGA fcc, GGA dhcp, and LDA fcc as shown in Figs. 9–11 following the RMTA discussed in Sec. II D. The spin-orbit interaction effect is negligible. All subsequent discussion, unless otherwise noted, refers to results for the β-fcc structure. The most pertinent data and its effect on the superconducting transition temperature are described in the following text. These data include the bulk modulus, the density of states DOS at ϵ_F, the Hopfield parameter η,[18] the electron-phonon coupling λ, the average phonon frequency ω, and the Coulomb pseudopotential $\mu*$ which was fixed at 0.13 for all calculations.

The bulk modulus from the GGA, LDA, and spin-orbit GGA is shown in Fig. 9 as a function of pressure. All three show small differences with pressure with the GGA and spin-orbit GGA following successively more linear trends. It is interesting that the GGA and LDA cross near 23 GPa,

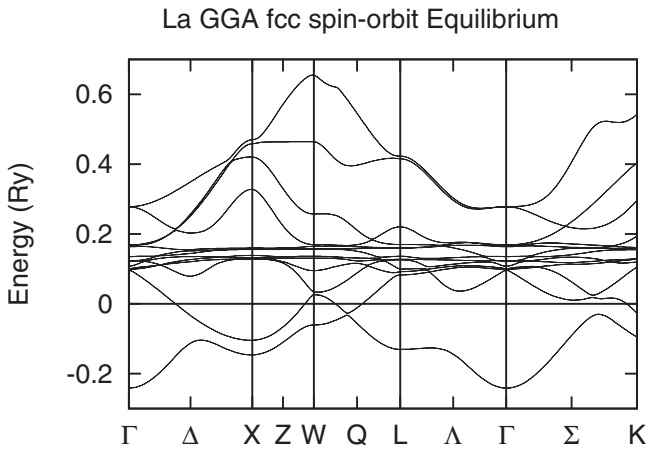

FIG. 8. Spin-orbit GGA fcc lanthanum at ambient pressure.

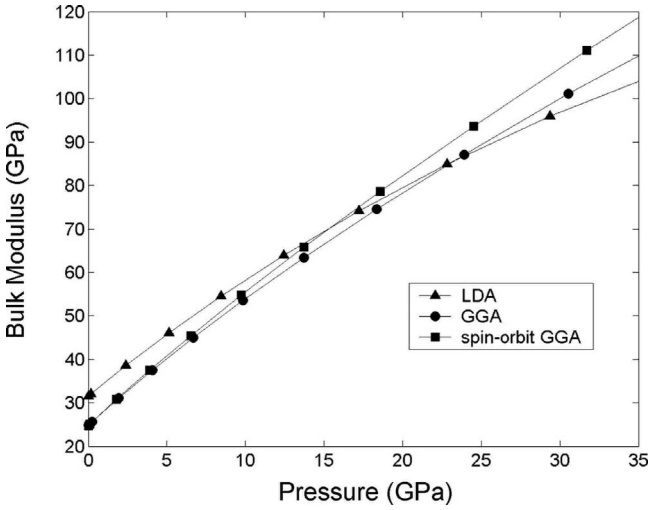

FIG. 9. Bulk modulus of GGA fcc lanthanum as a function of pressure.

where the experimental fcc ends. The average phonon frequencies show a similar trend, as displayed in Fig. 10, since they are roughly proportional to the bulk moduli. These trends, where B is roughly proportional to $\langle\omega\rangle$, also agree with those from similar investigations into the lighter third column elements of fcc yttrium[34] and fcc scandium.[35]

The variations in the density of states at the Fermi level $N(\epsilon_F)$, Hopfield parameter η,[18] and electron-phonon coupling λ with pressure are shown as functions of pressure in Figs. 11(a)–11(c), respectively. $N(\epsilon_F)$ remains constant with pressure up to about 10 GPa and then decreases, while η increases rapidly from 0 to 20 GPa. The maximum GGA η is 7.72 eV/Å^2 at 23.9 GPa, while the LDA reaches a maximum of 7.60 eV/Å^2 at slightly lower pressure. The η decreases after these pressures, reflecting the large influence of the d character of states at the Fermi level. Since the d-like states dictate the overall magnitude of electron-ion matrix element $\langle I^2\rangle$ and η is determined as the product of $\langle I^2\rangle$ and $N(\epsilon_F)$, the dominant $\langle I^2\rangle$ term yields a rapid increase in η

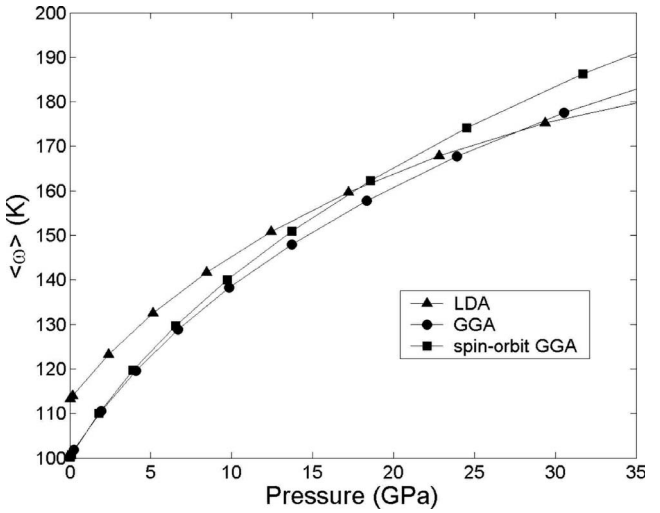

FIG. 10. Average phonon frequency $\langle\omega\rangle$ of GGA fcc lanthanum as a function of pressure.

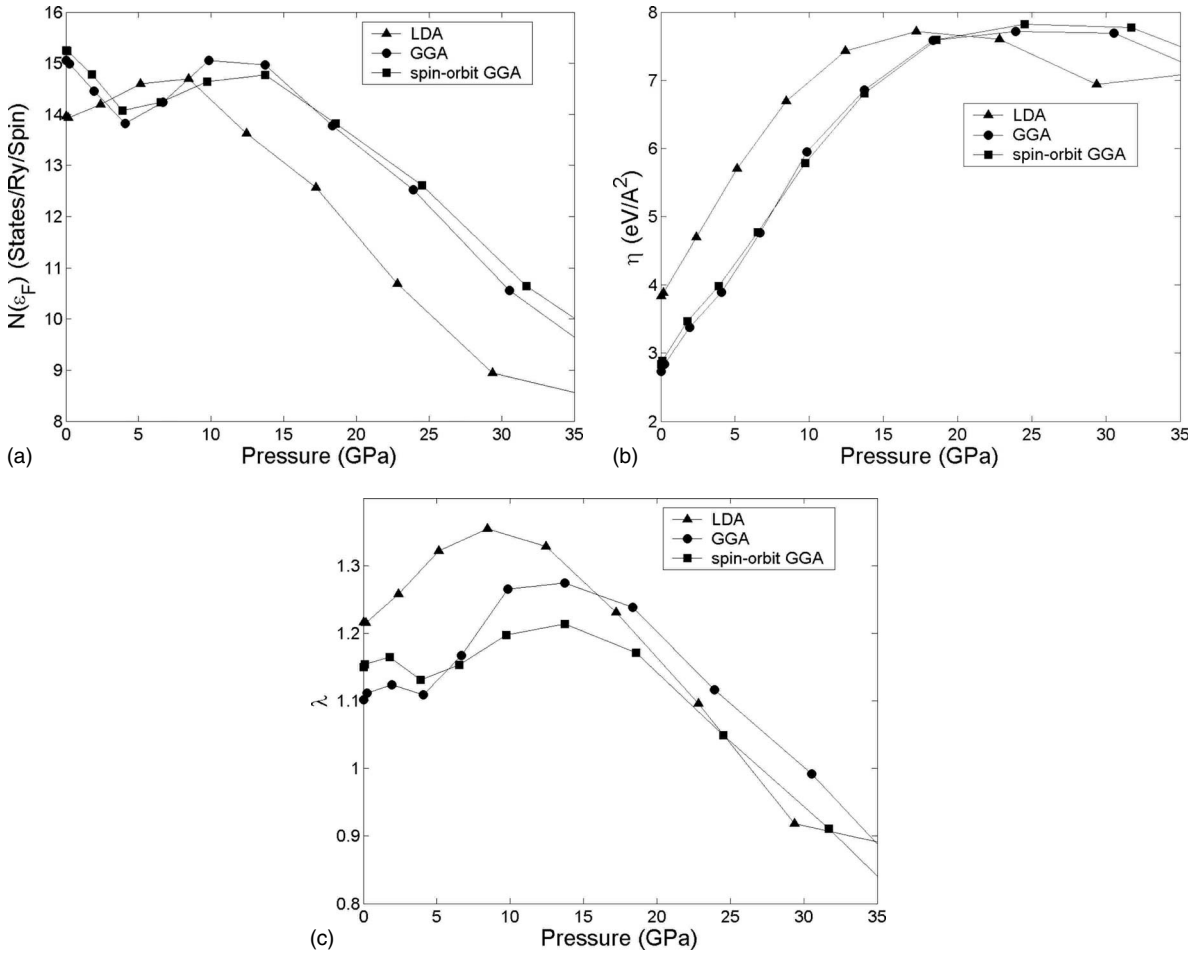

FIG. 11. $N(\epsilon_F)$, η, and λ of fcc lanthanum.

with pressure, and the η is maintained above 7 eV/Å^2 for more than half the pressure range.

The electron-phonon coupling λ increases with pressure, reaching maxima of 1.35 at 8.45 GPa in the LDA and 1.27 at 13.7 GPa in the GGA. At higher pressures, the calculated λ show a monotonic decrease with pressure. The GGA reaches a maximum T_c of 13.07 K at 18.34 GPa, which is a little more than 1.7% above experiment. The LDA achieves a higher maximum of 13.66 K at 12.44 GPa, overestimating experiment by more than 17%. Yet both the LDA and GGA exchange-correlation potentials, as shown in Fig. 12, capture the general fcc T_c trend from experiment. The experimental T_c data from Ref. 5 for the fcc and the distorted fcc (dfcc) structures are also shown for comparison.

We note that the spin-orbit interaction yields only small changes in the input parameters for the T_c calculations. The bulk modulus is higher in both the GGA and the LDA for pressures above 5 GPa when the spin-orbit interaction is included. This increased bulk modulus yields an increased average phonon frequency $\langle\omega\rangle$ which is not offset by the slightly increased Hopfield parameter η.[18] The electron-phonon coupling λ is decreased with the spin-orbit interaction, generating lower superconducting transition temperatures.

The calculated equilibrium GGA dhcp values were 24.39 GPa, 2.30 eV/Å^2, 0.83, and 106.27 and 4.36 K for the bulk modulus η, λ, $\langle\omega\rangle$, and T_c, respectively. We note a reduction in η and an increase in the average phonon frequency which yields a smaller electron-phonon coupling constant λ than that for the GGA fcc at ambient pressure. This reduced λ generates an equilibrium dhcp superconductivity transition

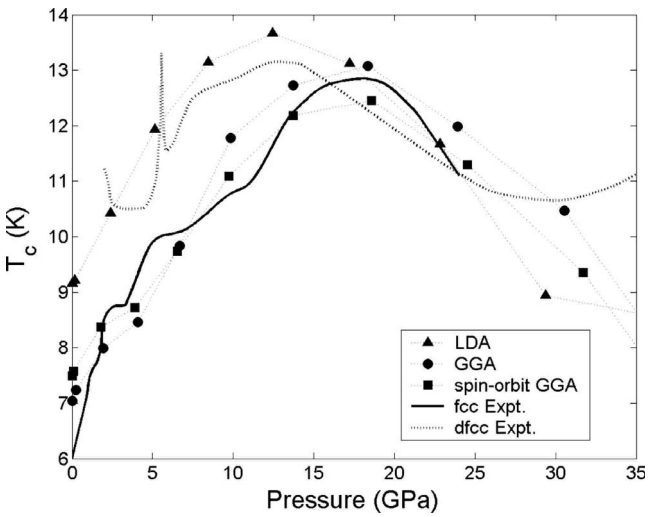

FIG. 12. Transition temperature T_c as a function of pressure for lanthanum. Experimental data are from Tissen *et al.* (Ref. 5).

TABLE V. Calculated and experimental phonon frequencies of equilibrium fcc lanthanum. (LAPW denotes linearized-augmented-plane-wave method and PP denotes pseudopotential method.)

q point	Coordinate	LAPW[a] (THz)	PP[b] (THz)	Expt.[c] (T=295 K) (THz)	(T=10 K) (THz)
Δ_1	(0.0, 0.0, 0.5)	1.67	2.03	2.01	2.06
X_3	(0.0, 0.0, 1.0)	2.76	2.81	2.96	2.95
W_2	(0.0, 0.5, 1.0)	1.77		1.92	2.00
Σ_1	(0.5, 0.5, 0.0)	1.81	2.20	2.24	2.18
L_2	(0.5, 0.5, 0.5)	2.42	2.25	2.67	2.61
Δ_5	(0.5, 0.0, 0.0)	1.48	1.62	1.58	1.65
X_5	(1.0, 0.0, 0.0)	2.07	2.21	2.13	2.24
W_5	(0.0, 0.5, 1.0)	1.64		2.32	2.23
Σ_2	(0.5, 0.5, 0.0)	1.37	1.55	1.34	1.38
Σ_3	(0.5, 0.5, 0.0)	2.11	2.34	2.16	2.27
L_3	(0.5, 0.5, 0.5)	0.70	0.85	0.86	0.78

[a]Present work, LAPW method using Perdew-Wang GGA.
[b]Reference 21, Vanderbilt GGA pseudopotential without 4f electrons.
[c]Reference 40, metastable fcc.

temperature of 4.36 K which is about 13.5% below the experimental value of 5.04 K.

To understand the origin of the variation in T_c with pressure we need to focus on the McMillan equations[33] [Eqs. (4) and (9)] for the electron-phonon coupling λ where T_c increases when $\langle\omega\rangle$ and λ increase. Indeed $\langle\omega\rangle$ increases with pressure but $\langle\omega\rangle$ also enters in the denominator of Eq. (4), which would have the effect of lowering λ. However, in the numerator of λ we have η which increases with pressure. Therefore, the increase in T_c with pressure up to 20 GPa does not have a simple explanation such as an increase in $N(\epsilon_F)$ or softening of the value of $\langle\omega\rangle$. The answer is more complicated. The increase in T_c up to 20 GPa and the subsequent fall is the result of an interplay of the interdependence among the values of λ, $\langle\omega\rangle$, and η.

F. Phonon frequencies

The phonon frequencies at high-symmetry q points were determined as functions of wave vectors using the frozen phonon approximation.[44] For each q point total energies were calculated as a function of the amplitude of a phonon wave using a unique k-point mesh consisting of 12 divisions from Γ to the high-symmetry q point, where each phonon wave was scaled such that the displaced atoms form a supercell. The phonon frequencies were then determined by the curvature of the energy from a second-order fit of the energy as a function of wave amplitude. Our results for GGA fcc lanthanum at equilibrium pressure are shown in Table V. Also shown are the corresponding results from Gao *et al.*[21] using density-functional perturbation theory (DFPT) (Ref. 45) and the room-temperature and low-temperature experimental results from Stassis *et al.*[40] All of our frequencies are below experiment except the room-temperature Σ_2 phonon, while about half of the DFPT results are below experiment.

Our results, like those using DFPT, compare best with experiment at room temperature. Here our Δ_1, Σ_1, W_5, and L_3 frequencies are more than 15% below experiment, while the L_2 and Σ_2 DFPT frequencies are about 15% below and above experiment, respectively. Comparing our results with experiment at low temperature we see the same four q points are more than 10% below experiment and the W_2 and Δ_5 frequencies are also more than 10% below experiment. The DFPT results are in better agreement with experiment with the L_2 and Σ_2 at about 14% and 12% below experiment, respectively.

Our calculated frequency at W_5 is more than 30% below experiment; we note that Gao *et al.*[21] were not able to reproduce the frequency dip seen from experiment at either this point or at the W_2 point. Still our other frequencies agree fairly well with both the DFPT results from Gao *et al.*[21] and experiment. Our frequencies, which are below experiment, are in qualitative agreement with our superconductivity T_c results using the RMTA. Specifically a smaller average frequency in the denominator of Eq. (4) would produce a larger electron-phonon coupling constant λ. This increase in λ would increase T_c such that the calculated equilibrium GGA fcc T_c would be slightly greater than experiment, about 1 K in our case, as our RMTA results predict.

IV. CONCLUSIONS

In conclusion, the electronic structure and superconductivity properties of lanthanum have been studied as functions of pressure using both the LDA and GGA forms of the exchange correlation within the LAPW method. In particular, we investigated the following: the total energies for the bcc, fcc, hcp, and dhcp structures; the elastic constants for the bcc and fcc at equilibrium conditions; the density of states, including spin-orbit interactions, for the fcc and GGA dhcp structures and the band structure for the GGA fcc; the superconducting properties, with spin-orbit interactions, for the fcc structure through high pressures and for the GGA dhcp structure at the calculated equilibrium; and the phonon spec-

trum for the GGA fcc structure at equilibrium conditions.

On the basis of total-energy and elastic constant calculations, the fcc structure has been shown to be stable at ambient conditions, while the bcc structure is unstable. Our GGA total-energy calculations agree very well with experiment, showing the correct phase ordering and the dhcp structure as energetically favorable at equilibrium. Total-energy calculations using the LDA though similar to those from other works are much less consistent with experiment, showing the fcc structure as energetically favorable.

Our density of states calculations show excellent agreement with previous LDA and GGA results for the fcc and dhcp structures. The spin-orbit interaction is shown to contribute little quantitatively to the total energy and density of states at the Fermi level. We see a notable qualitative difference in the spin-orbit and non-spin-orbit GGA fcc equilibrium band structures where the three triple-degenerate Γ bands split to form a double-degenerate and a nondegenerate band. Except for a notable difference in the bulk modulus, we see only minor changes due to spin-orbit interactions in the superconductivity properties for fcc lanthanum.

Finally our superconductivity calculations for LDA fcc and for GGA fcc and dhcp show very good agreement with experiment. The increase in λ, as shown in Eq. (4), comes from either an increase in η or a decrease in $M\langle\omega^2\rangle$ or a combination of the two. For pressures below 10 GPa, the large $N(\epsilon_F)$ is offset by the much smaller $\langle I^2\rangle$ in Eq. (5) so η is small. While the $N(\epsilon)$ stays relatively constant through 10 GPa $\langle I^2\rangle$ increases. Above 10 GPa $\langle I^2\rangle$ increases at a rate significantly greater than the decrease in $N(\epsilon_F)$. Therefore η increases rapidly with pressure and remains at or near a high value for more than half the pressure range.

The initial increase in λ comes from the rapid increase in η and the smaller average phonon frequencies $\langle\omega^2\rangle$. As pressure increases above 15 GPA η becomes relatively constant while $\langle\omega^2\rangle$ increases, decreasing λ. This decrease in λ causes the superconductivity transition temperature T_c to decrease even though $\langle\omega\rangle$ in the prefactor of Eq. (9) increases.

Both exchange-correlation potentials follow well the superconducting trend from experiment with the GGA showing the best agreement overall. Our phonon frequency calculations, which are in good agreement with other works and with experiment, are qualitatively consistent with our superconductivity results within the framework of the rigid-muffin-tin approximation.

[1] D. K. Finnemore, D. L. Johnson, J. E. Ostenson, F. H. Spedding, and B. J. Beaudry, Phys. Rev. **137**, A550 (1965).
[2] T. Jarlborg, G. Andersson, B. Sundqvist, and Ö. Rapp, J. Phys.: Condens. Matter **1**, 8407 (1989).
[3] H. Balster and J. Wittig, J. Low Temp. Phys. **21**, 377 (1975).
[4] J. Schilling, Physica C **460-462**, 182 (2007).
[5] V. G. Tissen, E. G. Ponyatovskii, M. V. Nefedova, F. Porsch, and W. B. Holzapfel, Phys. Rev. B **53**, 8238 (1996), and references within.
[6] J. Wittig, in *High Pressure in Science and Technology*, MRS Symposia Proceedings No. 22, edited by C. Homan, R. K. MacCrone, and E. Whalley, (North-Holland, Amsterdam, 1984), p. 17.
[7] G. S. Fleming, S. H. Liu, and T. L. Loucks, J. Appl. Phys. **40**, 1285 (1968).
[8] H. M. Myron and S. H. Liu, Phys. Rev. B **1**, 2414 (1970).
[9] E. A. Kmetko, in *Electronic Density of States*, Natl. Bur. Stand. (U.S.) Circ. No. 323, edited by L. H. Bennett (U.S. GPO, Washington, DC, 1971), p. 67.
[10] D. Glötzel and L. Fritsche, Phys. Status Solidi B **79**, 85 (1977).
[11] D. Glötzel, J. Phys. F: Met. Phys. **8**, L163 (1978).
[12] T. Takeda and J. Kubler, J. Phys. F: Met. Phys. **9**, 661 (1979).
[13] W. E. Pickett, A. J. Freeman, and D. D. Koelling, Phys. Rev. B **22**, 2695 (1980).
[14] A. K. McMahan, H. L. Skriver, and B. Johansson, Phys. Rev. B **23**, 5016 (1981).
[15] U. von Barth and L. Hedin, J. Phys. C **5**, 1629 (1972).
[16] Z. W. Lu, D. J. Singh, and H. Krakauer, Phys. Rev. B **39**, 4921 (1989).
[17] H. L. Skriver and I. Mertig, Phys. Rev. B **41**, 6553 (1990).
[18] J. J. Hopfield, Phys. Rev. **186**, 443 (1969).
[19] P. Söderlind, O. Eriksson, J. M. Wills, and A. M. Boring, Phys. Rev. B **48**, 9306 (1993).
[20] A. Delin, L. Fast, B. Johansson, O. Eriksson, and J. M. Wills, Phys. Rev. B **58**, 4345 (1998).
[21] G. Y. Gao, Y. L. Niu, T. Cui, L. J. Zhang, Y. Li, Y. Xie, Z. He, Y. M. Ma, and G. T. Zou, J. Phys.: Condens. Matter **19**, 425234 (2007).
[22] G. D. Gaspari and B. L. Gyorffy, Phys. Rev. Lett. **28**, 801 (1972).
[23] W. H. Butler, J. J. Olson, J. S. Faulkner, and B. L. Gyorffy, Phys. Rev. B **14**, 3823 (1976).
[24] S.-H. Wei and H. Krakauer, Phys. Rev. Lett. **55**, 1200 (1985).
[25] O. K. Andersen, Phys. Rev. B **12**, 3060 (1975).
[26] L. Hedin and B. L. Lundqvist, J. Phys. C **4**, 2064 (1971).
[27] J. P. Perdew and Y. Wang, Phys. Rev. B **45**, 13244 (1992).
[28] M. J. Mehl, B. M. Klein, and D. A. Papaconstantopoulos, *Intermetallic Compounds* (Wiley, London, 1994), Vol. 1.
[29] J. E. Osburn, M. J. Mehl, and B. M. Klein, Phys. Rev. B **43**, 1805 (1991).
[30] M. Born and K. Huang, *Dynamical Theory of Crystal Lattices* (Clarendon, Oxford, 1991), Chap. 11, p. 13.
[31] G. Lehmann and M. Taut, Phys. Status Solidi B **54**, 469 (1972).
[32] M. J. Gillan, J. Phys.: Condens. Matter **1**, 689 (1989).
[33] W. L. McMillan, Phys. Rev. **167**, 331 (1968).
[34] S. Lei, D. A. Papaconstantopoulos, and M. J. Mehl, Phys. Rev. B **75**, 024512 (2007).
[35] L. W. Nixon, D. A. Papaconstantopoulos, and M. J. Mehl, Phys. Rev. B **76**, 134512 (2007).
[36] H. L. Skriver and I. Mertig, Phys. Rev. B **32**, 4431 (1985).
[37] A. H. Daane, in *The Rare Earths*, edited by F. H. Spedding and A. H. Daane (Wiley, New York, 1961), p. 182.
[38] K. Syassen and W. B. Holzapfel, Solid State Commun. **16**, 533 (1975).

[39] C. Kittel, *Introduction to Solid State Physics*, 7th ed. (Wiley, New York, 1996), p. 59.
[40] C. Stassis, G. S. Smith, B. N. Harmon, K.-M. Ho, and Y. Chen, Phys. Rev. B **31**, 6298 (1985).
[41] C. Stassis, C.-K. Loong, and J. Zarestky, Phys. Rev. B **26**, 5426 (1982).
[42] D. L. Johnson and D. K. Finnemore, Phys. Rev. **158**, 376 (1967).
[43] P. H. Pan, D. K. Finnemore, A. J. Bevolo, H. R. Shanks, B. J. Beaudry, F. A. Schmidt, and G. C. Danielson, Phys. Rev. B **21**, 2809 (1980).
[44] B. M. Klein and R. E. Cohen, Phys. Rev. B **45**, 12405 (1992).
[45] S. Baroni, S. de Gironcoli, A. Dal Corso, and P. Gianozzi, Rev. Mod. Phys. **73**, 515 (2001).